ELSEVIER

Agricultural and Forest Meteorology 102 (2000) 275–286

AGRICULTURAL AND FOREST METEOROLOGY

www.elsevier.com/locate/agrformet

# Variation of net radiation over heterogeneous surfaces: measurements and simulation in a juniper–sagebrush ecosystem

Peter M. Anthoni [a,*], Beverly E. Law [b], Michael H. Unsworth [a], Richard J. Vong [a]

[a] *College of Oceanic and Atmospheric Sciences, Oregon State University, Corvallis, OR 97331, USA*
[b] *Department of Forest Science, Oregon State University, Corvallis, OR 97331, USA*

Received 5 May 1999; received in revised form 10 January 2000; accepted 14 January 2000

**Abstract**

As part of a larger study of carbon dioxide and energy exchange, energy components in an open-canopied juniper–sagebrush ecosystem located in the semi-arid region of Eastern Oregon were measured with the eddy covariance technique. Daytime net radiation averaged 20–30% greater than the sum of sensible, latent and soil heat fluxes. On cloudless days several days after a rain event the imbalance was ∼200–250 W m$^{-2}$. At such times, differences between the surface radiation temperatures of soil and foliage were large, and we investigated whether such differences may generate systematic errors in the measurement of net radiation.

A point measurement of net radiation above an open-canopied forest ecosystem is uncertain, because vegetation structure around the measurement location can be highly variable. Depending on location, various fractions of the upwelling radiation from the soil are intercepted by vegetation and do not reach the radiometer. To determine the magnitude of this uncertainty, we measured tree locations and dimensions, and surface radiation temperature ($T_r$) and shortwave reflection coefficients ($\alpha$) of soils and vegetation in a 100 by 100 m area. Geometrical models generated by ray tracing and rendering software were used to calculate the upwelling radiation that would reach radiometers placed at random locations above the surface.

In summer, under cloudless skies the measured radiative surface temperatures of soil and vegetation varied considerably, from a mean of 56°C for sunlit soil to 25°C for shaded soil, and 27–29°C for sunlit and shaded vegetation (trees and shrubs). The mean shortwave reflection coefficient varied little between components (with $\alpha_v$=0.10 for vegetation and $\alpha_s$=0.13 for soil).

Spatial variability in upwelling radiation ($R_u$) arises mainly from component variability at viewing angles from ∼30 to ∼60°, where contributions to $R_u$ are large and variation in fractional cover between radiometer locations is large. Our measurements and modeling suggest that a radiometer deployed from a tower in a small clearing will only be affected slightly by the clearing since only about 10% of $R_u$ arises from viewing angles less than 15° (directly below the radiometer).

The spatial variation in the upwelling radiation reaching a sensor above the canopy increases with increasing differences between the radiation temperatures and reflection coefficients of the various ecosystem components. For the radiative properties found at our site, where the radiative temperature of sunlit soil was ∼30°C larger than the temperature of vegetation and shaded components, the spatial variability in the longwave upwelling radiation ($R_{lu}$) was less than 20 W m$^{-2}$. The spatial variation in the shortwave upwelling radiation ($R_{su}$) for the small differences in the reflection coefficient of the ecosystem

*Corresponding author: Tel.: +541-737-2996; fax: 541-737-2540.
*E-mail address:* panthoni@oce.orst.edu (P.M. Anthoni)


PII: S0168-1923(00)00104-0

components was less than 10 W m$^{-2}$. Consequently, the uncertainty associated with estimating the available energy from a single point measurement of net radiation is not enough to explain the lack of energy closure (200–250 W m$^{-2}$) in this complex open-canopy ecosystem. 

*Keywords:* Eddy covariance; Energy budget; Net radiation; Reflection coefficient; Surface radiation temperature

## 1. Introduction

Net radiation is the driving term in the energy balance at the earth's surface, and is an essential component in widely used surface energy partitioning models (e.g. the Penman–Monteith equation by Monteith and Unsworth (1990)). In open-canopy ecosystems, net radiation is difficult to measure accurately. The energy exchange of short sparse vegetation is often modeled as a one-dimensional system with fluxes from two components, soil and plant canopy (Shuttleworth and Wallace, 1985). However, over tall vegetation the three-dimensional structure of the canopy has an important impact on the radiation distribution (Paw U, 1992). For example, the overstory vegetation can intercept reflected shortwave and emitted longwave radiation from the soil surface, and the fraction of the soil surface that is shaded from direct radiation varies with solar elevation, azimuth and overstory structure.

Many surface-atmosphere energy exchange studies have been undertaken over relatively homogeneous canopies, where micro-scale variations in canopy structure are small compared to the source area contributing to measured energy fluxes. In most flux studies, instrumentation is installed above the canopy at one location. Sensible and latent heat fluxes typically are measured with the eddy covariance technique, and a net radiometer measures the difference between upward and downward long- and shortwave radiation. Heat flux into or out of the soil is usually measured with heat flux plates buried underneath the soil surface. In addition, rates of temperature change in the canopy air layer and biomass of the ecosystem components (e.g. tree stems, leaves) are used to determine the energy storage below the measurement level.

Achievement of energy closure is generally used to test the validity of the eddy covariance technique in measuring atmosphere-surface exchange (Goulden et al., 1996). Usually a one-dimensional energy budget is applied, where available energy, calculated from net radiation ($R_n$) minus soil heat flux ($G$), should be balanced by the algebraic sum of sensible heat ($H$), latent heat (LE), and change in energy storage in the ecosystem ($S$). Horizontal advection effects are usually minimized by careful selection of a research site with uniform fetch in the prevailing wind directions.

In summer of 1997 we made measurements of the energy exchange over an open-canopied juniper–sagebrush ecosystem using eddy covariance instrumentation. At our site an energy imbalance of 200–250 W m$^{-2}$ occurred on cloudless summer days when differences between surface radiation temperatures were found to be largest (unpublished data). Our ability to account for only about 70–80% of the available energy was relatively low compared with values reported for denser forest ecosystems (∼80–100%; Kelliher et al., 1992; Lee and Black, 1993; Laubach et al., 1994; Fan et al., 1995; Goulden et al., 1996; Blanken et al., 1997; Grelle, 1997; McCaughey et al., 1997). Lack of closure at our site could be partly due to neglect of advection effects (i.e., mesoscale transfer), errors in the estimation of soil heat flux and soil heat storage, uncertainties in the calibration of the net radiometer, errors in the measurements of eddy fluxes, and uncertainty in assessing the appropriate spatial mean net radiation. The estimation of $R_n$ using a single net radiometer at heterogeneous semi-arid sites may be biased because of spatial variation in the surrounding vegetation.

At several boreal flux sites net radiation measured from towers compared well with spatial average $R_n$ estimated from aircraft data (Desjardins et al., 1997). However, spatial variation in $R_n$ at the boreal sites can be expected to be smaller than at our site, because of the relatively large leaf area (leaf area index (LAI) of 1.8 to 5.6 with a mean of 3), large stand density (980 to 15160 trees/ha with a mean of 5000 trees/ha), and most likely small differences in surface radiation temperatures of the main ecosystem components since boreal soils are covered by moss or other understory species (Gower et al., 1997). The stand characteristics of the boreal sites are in strong contrast to our

semi-arid, open-canopied juniper–sagebrush ecosystem with LAI<1, stand density of 128 trees/ha, and soil temperatures exceeding vegetation temperature by many degrees on cloudless summer days.

In this paper, we assess the magnitude of uncertainty in net radiation at our site, by combining measurements and modeling to estimate spatial variability in the upwelling shortwave and longwave radiation. To determine the spatial variation in the surface and vegetation cover, we measured tree locations and dimensions, and surface radiation temperature ($T_r$), and solar reflection coefficients ($\alpha$) of soils and plant species in a 100 by 100 m area. We then used geometrical models, generated by ray tracing and rendering software, to calculate the upwelling radiation reaching randomly selected radiometer locations above the surface.

## 2. Methods

### 2.1. Site description

Components of the energy exchange and associated microclimatic variables were measured above the canopy of a juniper–sagebrush ecosystem located about 15 km east of Sisters, Oregon (44°15′54″N, 121°23′3″ W, elevation 945 m). The site is about 3 km southwest of a Juniper research site studied during the Oregon Transect Ecosystem Research (OTTER) project for which details of the ecosystem and its physiology were reported by Runyon et al. (1994) and Law and Waring (1994). The fetch is relatively flat and uniform for several kilometers in all wind directions. The overstory consists primarily of widely-dispersed juniper trees (*Juniperus occidentalis*) and has a spatial mean leaf area index (LAI) of less than 1. The understory consists of sagebrush (*Artemisia tridentata*), rabbit brush (*Chrysothamnus viscidiflorus*), bitterbrush (*Purshia tridentata*), and a small percentage of various grass species. The well drained sandy loam soils are classified as coarse-loamy, mixed, mesic aridic Haploxeroll (USDA, National Soil Survey Center, Soil Survey Laboratory).

### 2.2. Microclimate measurements

Above-canopy meteorological measurements were recorded at the top of the tower (∼20 m above the surface), using a Campbell Scientific (CSI, Logan, UT) datalogger. Above-canopy net radiation ($R_n$) was measured with a net radiometer (model Q7, REBS, Seattle, WA, with factory calibration dated December 12, 1996), deployed from the south side of the tower. Net radiation was corrected for the influence of wind speed, using an equation supplied by the manufacturer. Downward photosynthetically active radiation (PAR) was measured with quantum sensor (model LI-190SZ, LI-COR Inc, Lincoln, NE). Incoming total solar radiation ($S_t$) was estimated from measured PAR, using a conversion factor of 0.5 for cloudless skies determined from $S_t$ and PAR measured at a nearby ponderosa pine site (20 km West of the juniper site). Air temperature ($T_a$) and relative humidity (RH) were measured with a thermistor and capacitive RH sensor probe (model HMP35C, Vaisala, Helsinki, Finland).

Various other measurements were recorded at ground level using CSI dataloggers. Soil heat flux was measured at 0.02 m depth with two heat flux plates (model HFT-3, REBS, Seattle, WA), one at the north and the other at the south side of a Juniper tree. The heat fluxes at the two locations were equally weighted to estimate the soil heat flux for the ecosystem. Soil temperature was measured next to the heat flux plates with thermocouples at depths of 2, 16, and 32 cm. Rainfall was measured with a tipping-bucket rain gauge (model TE525MM, Campbell Scientific, Inc., Logan, UT), placed at least 5 m from surrounding trees.

### 2.3. Intensive mensuration plot

A 100 m × 100 m area in the typical upwind fetch of the eddy covariance system was divided into 10 m × 10 m cells. In each cell the *x*–*y* locations of trees with a diameter at breast height >7 cm were recorded. The total height of each tree and height to the base of live crown was measured with an inclinometer, and maximum crown radius was also recorded. Percentage cover estimates of the major ecosystem components (soil, juniper trees, shrubs, and grasses) were determined by the line intercept method on two 100 m long transects located within the 100 m × 100 m area.

Leaf area index measurements were made with a LAI-2000 plant canopy analyzer (LICOR, Lincoln, NE) in July after full needle expansion. Measurements were made under uniform diffuse light conditions at

10 m grid points ($n$=121 sample points). We used a 90° view restrictor to block the view of the operator, and to account for canopy gaps. The LAI-2000 was held at the soil level at each measurement point. A second LAI-2000 was located as a reference on top of the flux tower above the canopy. The instruments were synchronized and calibrated to one another prior to the measurements.

### 2.4. Measurements of surface properties of ecosystem components

During two cloudless days in summer 1997, measurements of longwave radiation emitted from individual surface components inside the 100 m×100 m plot were made with a handheld infrared radiation (IR) thermometer (model 43, Telatemp, Fullerton, CA). The instrument was calibrated prior to the field measurements over a well stirred water bath at several water temperatures.

The total upwelling longwave radiation ($R_{lu}$) originating from a surface is given by (Huband and Monteith, 1986)

$$R_{lu} = \varepsilon_s \sigma T_r^4 + (1 - \varepsilon_s) R_{ld} \quad (1)$$

where $\varepsilon_s$ is the surface emissivity, $\sigma$ is the Stefan–Boltzman constant (5.67E-8 W m$^{-2}$ K$^{-4}$) and $T_r$ is the surface radiation temperature, $R_{ld}$ is the downwelling longwave radiation. An IR thermometer will observe the total upwelling radiation and report an apparent surface radiation temperature ($T_{ar}$), determined by

$$R_{lu} = \sigma T_{ar}^4 \quad (2)$$

Hence the surface radiation temperature $T_r$ of the surface component can be calculated by

$$T_r = \left[ \frac{1}{\varepsilon_s \sigma} (\sigma T_{ar}^4 - (1 - \varepsilon_s) R_{ld}) \right]^{1/4} \quad (3)$$

For our modeling purposes we were interested in the total upwelling radiation originating from the main surface components (sunlit and shaded soil and vegetation). Apparent surface radiation temperatures were measured for surface components at several locations during the day (9:00–16:00 local time). Surface radiation temperatures for sunlit soil ($T_{r,s,su}$), shaded soil ($T_{r,s,sh}$), sunlit vegetation ($T_{r,v,su}$), and shaded vegetation ($T_{r,v,sh}$) were calculated from measured $T_{ar}$ using Eq. (3); $R_{ld}$ for cloudless skies was modeled from measured air temperature ($T_a$) at 20 m, according to $R_{ld}$=−119+1.06 $\sigma T_a{}^4$ (Unsworth and Monteith, 1975). Surface emissivities were taken to be 0.93 for soil and 0.97 for vegetation (Hipps, 1989; Humes et al., 1994).

Shortwave reflection coefficients were measured with an Eppley pyranometer (model PSP, Eppley laboratory, Newport, Rhode Island). The pyranometer was held above the various ecosystem components at a height of ∼1 m facing downward to measure the reflected shortwave radiation, and was then reversed and leveled to measure the incoming shortwave radiation. Reflection coefficients were measured for soil ($\alpha_s$) and vegetation (shrubs and juniper trees; $\alpha_v$) at several locations during the day (9:00–16:00 local time).

### 2.5. Modeling of the radiometer field of view

We used the 100 m×100 m plot information and ray tracing software (Blue Moon Rendering Tools; Gritz and Hahn, 1996) to generate scenes that would be viewed by a radiometer located 20 m above the surface and facing downward. The measured tree pattern of the 100 m×100 m area was repeated outward in the model to generate a larger scene that allowed a viewing angle ($\phi$) of at least 85° in all directions, sufficient to capture 99% of the upwelling radiation contributions (Schmid, 1997). Trees were modeled as paraboloids. Because shrub locations were not measured explicitly in the 100 m×100 m plot, we accounted for the shrub cover by randomly locating half-spheres with a radius of 1 m into the modeled scenes until the area covered was equal to the percent cover for shrubs determined from line intercept method. We did not include the small percentage of grasses in the modeling, as they had senesced by the time we made the radiation measurements.

For each of 100 random instrument locations within the plot, scenes with a pixel size of 1 m×1 m were generated. Vegetation and soil were assigned different pixel colors. Fig. 1 shows an orthogonal view of the 100 m×100 m area and a perspective view of the same area as seen from a radiometer placed at 20 m above the surface in the center of the area. Sun position in

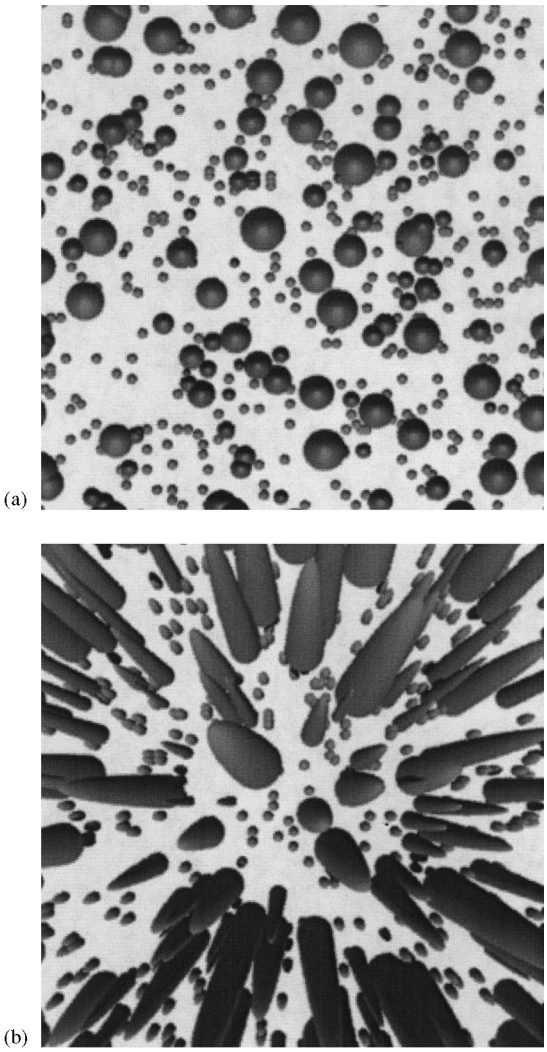

Fig. 1. (a) Orthogonal view of the 100 m×100 m plot with known tree location and dimensions. (b) View of the same area as seen from the perspective of a radiometer located at a height of 20 m above the surface. The views were generated with BMRT ray tracing software; trees were modeled as paraboloids, shrubs were modeled as half-spheres, and the sun was at an elevation of 65° around solar noon. For image clarity, trees and shrubs were modeled without casting a shadow onto the soil in these scenes.

the images corresponded to solar noon in mid-summer (elevation ~65°), corresponding to the middle of the period over which surface radiation properties were measured in the 100 m×100 m area. Sunlit and shaded areas were distinguished by different pixel shades (e.g. bright pixels were sunlit and dark pixels shaded).

### 2.6. Calculation of upwelling longwave and shortwave radiation

In each scene, the fractions of sunlit ($f_{s.su}$) and shaded soil ($f_{s.sh}$) and sunlit ($f_{v.su}$) and shaded ($f_{v.sh}$) vegetation were determined from pixel colors and shades in concentric rings centered on the radiometer location. Taking into account the interception of radiation by the overstory, the upwelling longwave radiation ($R_{lu.3D}$) received by the radiometer can be calculated from fractional surface cover and the component-specific upwelling radiation calculated from the measured surface radiation temperature of the sunlit and shaded soil and vegetation (Schwerdtfeger, 1976),

$$R_{lu.3D} = 2\Sigma_m \Sigma_i \sin(\phi_i)\cos(\phi_i)\delta\phi_i R_{lu,m} f_{m,i} \quad (4)$$

where $\phi_i$ is the mean viewing angle of the $i$th concentric ring ($n$=150), $\delta\phi_i$ is the width of the concentric ring in radians (see Fig. 2), $\sigma$ is the Stefan–Boltzman constant (5.67E–8 W m$^{-2}$ K$^{-4}$) and $R_{lu,m}$ ($=\sigma T^4_{ar,m}=\varepsilon_s \sigma T^4_{r,m}+(1-\varepsilon_s)\ R_{ld}$) is the total upwelling longwave radiation of the $m^{th}$ surface component (e.g., sunlit soil, shaded soil, sunlit vegetation, and shaded vegetation) with fractional viewing cover of $f_{m,i}$ in the $i^{th}$ concentric ring.

Similarly, the reflected solar radiation ($R_{su.3D}$) was determined using the measured reflection coefficients of the soil and vegetation. Total incoming solar radiation ($S_t$) was set at 900 W m$^{-2}$, a representative value measured around solar noon on cloudless sum-

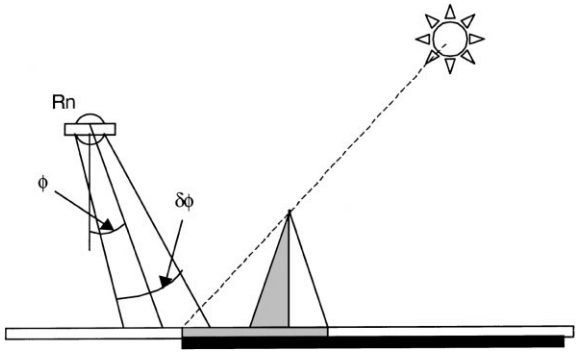


Fig. 2. View schematic of radiometer over a surface with three dimensional structure. Shaded areas are shown in gray. The apparent area seen as shade by the radiometer is shown in black.

mer days at this site. For reflection of diffuse radiation ($S_d$) by shaded areas, we estimated $S_d$ to be 0.1 of $S_t$ for cloudless days (Monteith and Unsworth, 1990). $R_{su.3D}$ received by the radiometer is then given by

$$R_{su.3D} = 2\Sigma_i(\sin(\phi_i)\cos(\phi_i))\delta\phi_i\left(\Sigma_{su}\alpha_{su}S_t f_{su,i} + \Sigma_{sh}S_d\alpha_{sh}f_{sh,i}\right) \quad (5)$$

where $\phi_i$ is the mean viewing angle of the $i^{th}$ concentric ring ($n$=150), $\delta\phi_i$ is the width of the concentric ring in radians, $S_t$ is the total incoming radiation, $S_d$ is the diffuse radiation, 'su' and 'sh' are the sunlit and shaded components of the ecosystem, respectively, $\alpha_{su}$ and $\alpha_{sh}$ are the reflection coefficients, and $f_{su,i}$ and $f_{sh,i}$ are the fraction covers of the scene components in the $i^{th}$ concentric ring.

Taking into account the dependence of the vegetation fraction on viewing angle, the average vegetation fraction viewed by a radiometer as a function of viewing angle can be expressed as (Norman et al., 1995)

$$f_{v.av} = 1 - \exp\left(-k\frac{LAI}{\cos(\phi)}\right) \quad (6)$$

where $k$ is a light extinction coefficient, LAI is the leaf area index, and $\phi$ is the viewing angle. The average upwelling longwave ($R_{lu.av}$) and shortwave radiation ($R_{su.av}$) were then calculated using equations similar to (4) and (5) with vegetation cover fraction $f_v$ calculated from $f_{v.av}(\phi_i)$ and soil cover fraction $f_s$=1−$f_{v.av}(\phi_i)$, together with an estimate of the shaded to sunlit fraction of the ecosystem. We estimated the shaded to sunlit fractions from the ratios of the orthogonal percentage cover fractions of the shaded and sunlit components (soil and vegetation).

Dolman (1993) suggested calculating the available energy for open-canopy ecosystem based on the fractional cover of understory and overstory. This two-dimensional approach neglects interception of upwelling radiation by three-dimensional structures. We calculated the longwave upwelling radiation ($R_{lu.2D}$) using this approach, according to

$$R_{lu.2D} = \Sigma_m R_{lu,m} f_m \quad (7)$$

where $\sigma$ is the Stefan–Boltzman constant, and $R_{lu,m}$ ($=\sigma T_{ar,m}^4 = \varepsilon_s\sigma T_{r,m}^4 + (1-\varepsilon_s)R_{ld}$) is the total upwelling longwave radiation and $f_m$ is the vertically projected fraction cover of the $m^{th}$ surface component (e.g., sunlit soil, shaded soil, sunlit vegetation, and shaded vegetation).

Similarly, a two-dimensional estimate of upwelling shortwave radiation ($R_{su.2D}$) was calculated as,

$$R_{su.2D} = \Sigma_{su}\alpha_{su}S_t f_{su} + \Sigma_{sh}\alpha_{sh}S_d f_{sh} \quad (8)$$

where $S_t$ is the total incoming radiation, $S_d$ is the diffuse radiation, $\alpha_{su}$ and $\alpha_{sh}$ are the reflection coefficients, and $f_{su}$ and $f_{sh}$ are the vertically projected fractional cover of the 'su' (sunlit soil and vegetation) and 'sh' (shaded soil and vegetation) components of the ecosystem.

## 3. Results and discussions

### 3.1. Intensive mensuration measurements

There were 128 juniper trees in the 100 m×100 m plot. The mean height of the trees was ∼7 m, and mean spacing between the trees, calculated from the mean distance of the five closest neighbors of each tree in the plot, was about 9 m. Percent cover estimates from line intercept method were: 60% bare soil; 24% Juniper; 11% shrubs; and 5% grasses and other species. The vegetation percentage cover at our site is higher than at the nearby OTTER site, which had 7% juniper and 13% shrubs, estimated in the same way (Law and Waring, 1994). An analysis of the orthogonal view of the 100 m×100 m scene (Fig. 1a) modeled with the sun at noon and elevation of 65°, showed that 58% of the area would be sunlit soil, 9% shaded soil, 21% sunlit vegetation, and 12% shaded vegetation. Some overlap of the randomly-placed shrubs with juniper trees occurred in the modeled view scenes, which resulted in a tree and shrub percentage slightly lower than was found from the line intercept method.

### 3.2. Environmental conditions and energy closure

Skies were cloudless during the measurements of surface radiation temperatures and the reflection coefficients of the various ecosystem components in the 100 m×100 m plot. At the tower, midday solar radiation reached values of ∼900 W m$^{-2}$ and net radiation was about 650–700 W m$^{-2}$. Midday air temperature was ∼23°C, and soil temperatures measured at 2 cm

Table 1
Mean surface radiation temperatures ($T_r$) and standard errors () for the major ecosystem components[a]

| Type | Mean $T_r$, (SE) in °C | $N$ |
|---|---|---|
| Soil (sunlit) | 56 (0.7) | 12 |
| Soil (shade) | 25 (1.1) | 9 |
| Juniper (sunlit) | 29 (0.9) | 15 |
| Juniper (shade) | 27 (1.2) | 6 |
| Shrubs (sunlit) | 28 (0.5) | 26 |
| Grass (sunlit) | 60 (1.3) | 2 |
| Grass (shade) | 30 (3.2) | 3 |

[a] Measurements were performed from 9:00 to 16:00 local time during two cloudless days in summer of 1997 (Day 203–204). $T_r$ was calculated from measured $T_{ar}$ using Eq. (3); $N$ is the number of samples taken for each surface type.

depth were ∼40 and ∼20°C at the sunlit and shaded side of a tree, respectively. Measured surface radiation temperature varied considerable between soil and vegetation (Table 1). The measured mean total upwelling longwave radiation was ∼640 W m$^{-2}$ for sunlit bare soil ($R_{lu,s,su}$), ∼440 W m$^{-2}$ for shaded soil ($R_{lu,s,sh}$) and ∼460–470 W m$^{-2}$ for the dominant vegetation ($R_{lu,v,su}$ and $R_{lu,v,sh}$). A similar pattern of surface radiation, with $T_r$ of sunlit areas substantially higher than $T_r$ of vegetation, has been reported at other research sites (Garratt, 1978; Blyth and Harding, 1995). Reflection coefficients differed little between vegetation and soil (Table 2). At a semi-arid site located in Idaho, Dirmhirn and Belt (1971) found higher reflectivity for shrubs (0.12–0.15) and soil (0.20) than at our site. The lower measured reflection coefficient of vegetation at our site may have been due to the influence of the underlying soil. Compared to reflection coefficients of dry soils ($\alpha$=0.19±0.06) (Jones, 1992, p. 31) our measured soil reflection coefficient was relatively low.

Table 2
Measured mean reflection coefficient (a) and standard error () of the major ecosystem components[a]

| Type | Mean $\alpha$ (SE) | $N$ |
|---|---|---|
| Soil | 0.13 (0.013) | 6 |
| Juniper | 0.10 (0.002) | 30 |
| Shrubs | 0.11 (0.003) | 52 |

[a] Measurements were performed from 9:00 to 16:00 local time during two cloudless days in summer of 1997 (Day 203–204). $N$ is the number of samples taken for each surface type.

### 3.3. Modeled upwelling longwave and shortwave radiation

In the simulations, the variation in the vegetation fraction viewed by the randomly placed radiometers ($f_v$=$f_{v,su}$+$f_{v,sh}$; Fig. 3) was large for viewing angles less than 15°, and decreased with increasing viewing angle. At all locations, $f_v$ increased, and consequently $f_s$(=1−$f_v$) decreased, for larger viewing angles until vegetation dominated the field of view. The relation between the vegetation fraction in the field of view of a radiometer and viewing angle ($\phi$) is given by Eq. (6). Assuming a random leaf distribution with an extinction coefficient $k$=0.5, the best fit of the Eq. (6) to the data in Fig. 3 is for a LAI of 0.81 ($r^2$=0.91, Fig. 3). This estimate agrees very well with our measured mean LAI of 0.77 (SE 0.06, $n$=121) in the 100 m×100 m plot.

Fig. 4 shows the contributions from different viewing angles to total (short+longwave) upwelling radiation ($R_{u.3D}$=$R_{su.3D}$+$R_{lu.3D}$) as a function of viewing angle for each of the 100 randomly-placed simulated radiometer locations. The highest contributions to $R_{u.3D}$ were from viewing angles around 45°. The variations in $R_{u.3D}$ were small for viewing angles less than 15° and greater than 70°. Areas with viewing angles of <15°, <42°, and <70° (corresponding to radial distances of 5, 18, and 55 m from the center)

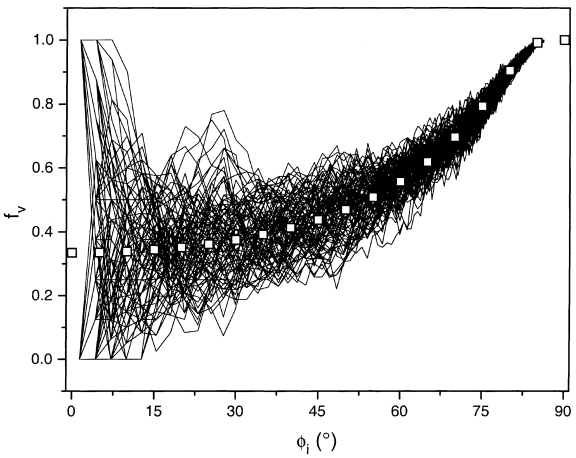


Fig. 3. Vegetation fraction ($f_v$) versus viewing angle ($\phi$) for all randomly-placed simulated radiometer locations. A fit of the average vegetation fraction viewed by a radiometer as a function of viewing angle (Eq. (6)) is shown with open square symbols.

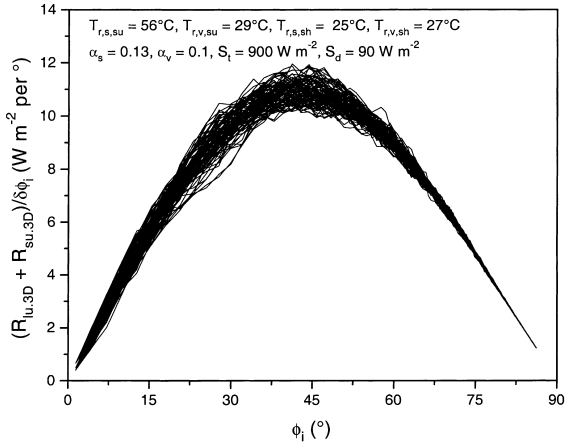


Fig. 4. Contributions to the upwelling radiation ($R_u$=$R_{lu}$+$R_{su}$) versus originating viewing angle ($\phi$) for all random radiometer locations.

contributed 10, 50, and 90% of the upwelling radiation, respectively, which is in agreement with findings by Schmid (1997). The modeled scenes encompassed a viewing angle of up to 86°; contributions to $R_u$ from larger angles than this are expected to be less than 0.5% of $R_u$, as can be estimated from Fig. 4. Large variations in soil and vegetation fractions occurred close to the simulated radiometer locations but their contributions to the upward radiation are small since the area is small (sine weighting in Eqs. (4) and (5)). Variation in cover fraction decreases with higher viewing angles until the radiometer views mainly vegetation, and contributions from the soil become less important (Fig. 3). The main cause of spatial variation in $R_u$ arises from component variability at viewing angles from ∼30 to ∼60°, where contributions to $R_u$ are high and variation in fractional cover between radiometer locations is large. Fig. 3 and Fig. 4 indicate that a radiometer deployed from a tower in a small clearing will only be affected slightly by the clearing, since only about 10% of $R_u$ arises from viewing angles less than 15°.

The simple 2-D scaling of the upward radiation according to percent cover fraction (estimated from Fig. 1a) (i.e. neglecting the three dimensional structure of the surface), and using representative values of $T_r$ ($T_{r,s,su}$=56°C; $T_{r,s,sh}$=25°C; $T_{r,v,su}$=29°C; $T_{r,v,sh}$=27°C) for cloudless summer conditions and $\alpha_s$=0.13 for soil and $\alpha_v$=0.10 for vegetation resulted in $R_{lu.2D}$=566 W m$^{-2}$ and $R_{su.2D}$=88 W m$^{-2}$. With the 3-D scaling, based on 100 randomly-placed simulated radiometers above the ecosystem, the mean values of $R_{lu.3D}$ and $R_{su.3D}$ were 534 W m$^{-2}$ (SD 6.4) and 76 W m$^{-2}$ (SD 2.7) respectively, both significantly lower (6 and 14%) than the 2-D scaling estimates. By taking into account the change in vegetation fraction with viewing angle (Eq. (6) with $k$=0.5 and LAI=0.81), $R_{lu.av}$ and $R_{su.av}$ would be 543 and 82 W m$^{-2}$, respectively, slightly higher than the $R_{lu.3D}$ and $R_{su.3D}$.

We determined the sensitivity of $R_{lu}$ to differences in $T_r$ between the sunlit ecosystem components, by varying one $T_r$ (i.e., that of sunlit soil or sunlit vegetation) while holding the other fixed at 29°C (Fig. 5). For both cases, the shaded soil and shaded vegetation were assigned $T_r$ values of 25 and 27°C, respectively. The range of $R_{lu.3D}$ increased with increasing differences in the surface radiation temperatures of the ecosystem components (Fig. 5). For temperature differences between $T_{r,s,su}$ and $T_{r,v,su}$ in excess of ∼5 K, the range in $R_{lu.3D}$ was higher for the case of varying $T_{r,s,su}$ (Fig. 5a) than for the case of varying $T_{r,v,su}$ (Fig. 5b). Fig. 5 shows that even for high temperature differences between soil and vegetation the uncertainty in $R_{lu}$ due to a single point estimate is less than ∼20 W m$^{-2}$. This uncertainty is small compared to the energy imbalance of ∼200–250 W m$^{-2}$ on days when the difference between temperatures of sunlit soil and vegetation was large.

Fig. 5 also show the 2-D estimates of $R_{lu.2D}$ for varying $T_r$. For our ecosystem, with larger soil percent cover than vegetation cover, the orthogonal percent cover fraction of sunlit soil was larger than the soil fraction seen by the 100 random radiometers. Therefore, $R_{lu.2D}$ increased with $T_{r,s,su}$ more than any of the $R_{lu.3D}$ values (Fig. 5a), and increased less with $T_{r,v,su}$ than any of the $R_{lu.3D}$ values, but fell within the range of $R_{lu.3D}$ for $T_{r,v,su}$>35°C (Fig. 5b). The 2-D and 3-D estimates of the upwelling longwave radiation are similar only for small differences between the soil and vegetation radiation temperatures or when $T_{r,v,su}$is larger than $T_{r,s,su}$. When $T_{r,s,su}$ is larger than $T_{r,v,su}$, the 2-D approach always results in an overestimate of the upwelling longwave radiation.

Similarly, we determined the sensitivity of $R_{su}$ to differences in the reflection coefficients between the soil and vegetation, by varying either $\alpha_s$ or $\alpha_v$ while

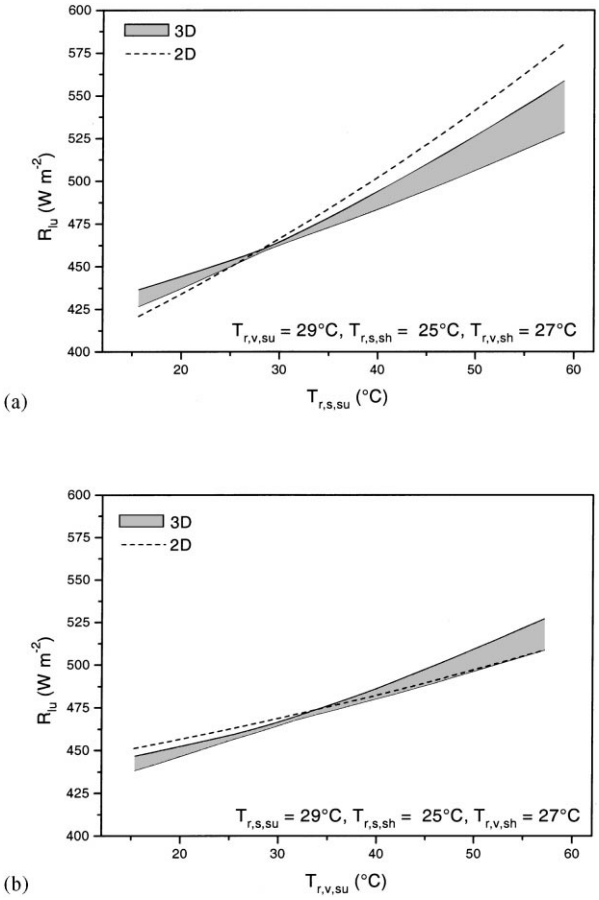


Fig. 5. Range in the modeled upwelling longwave radiation, $R_{lu.3D}$, of the 100 randomly-placed simulated radiometer locations versus varying surface radiation temperature of (a) sunlit soil ($T_{r,s,su}$) and (b) sunlit vegetation ($T_{r,v,su}$). The 2-D estimate of $R_{lu.2D}$ is shown as a dashed line.

holding the other fixed at 0.1 (Fig. 6). $S_t$ and $S_d$ were specified as 900 and 90 W m$^{-2}$ respectively. The range in $R_{su.3D}$ increased with increasing difference between the ecosystem reflection coefficients, and was higher for the case of varying $\alpha_s$ (Fig. 6a) than varying $\alpha_v$ (Fig. 6b). Fig. 6 shows that even for large differences in the reflection coefficients between soil and vegetation the uncertainty in $R_{su}$ due to a single point estimate is less than ~25 W m$^{-2}$. As for $R_{lu.2D}$ and $R_{lu.3D}$, $R_{su.2D}$ increased with $\alpha_s$ more than any of the $R_{su.3D}$ values (Fig. 6a) and increased less with $\alpha_v$ than any of the $R_{su.3D}$ values, but fell within the range of $R_{su.3D}$ for $\alpha_v$>0.15 (Fig. 6b). The 2-D and 3-D estimates of $R_{su}$ will be similar for ecosystems with small differences between reflection coefficients or when $\alpha_v$ is larger than $\alpha_s$, but a 2-D analysis will result in an overestimate of the upwelling shortwave radiation for the case when $\alpha_s$ is larger than $\alpha_v$.

Radiation emitted from the soil and blocked by vegetation becomes important for viewing angles higher than 45° (Fig. 3). We found a difference of ~30 W m$^{-2}$ between the mean $R_{lu.3D}$ and $R_{lu.2D,}$ for the case where the temperature difference between soil and vegetation was ~25–30 K. The difference between the mean $R_{su.3D}$ and $R_{su.2D}$ was ~15 W m$^{-2}$ when the soil reflection coefficient (0.13) was slightly higher than the vegetation reflection coefficient (0.10). This indicates that ignoring the 3-D blocking effect may result in erroneous estimates of upwelling radiation.

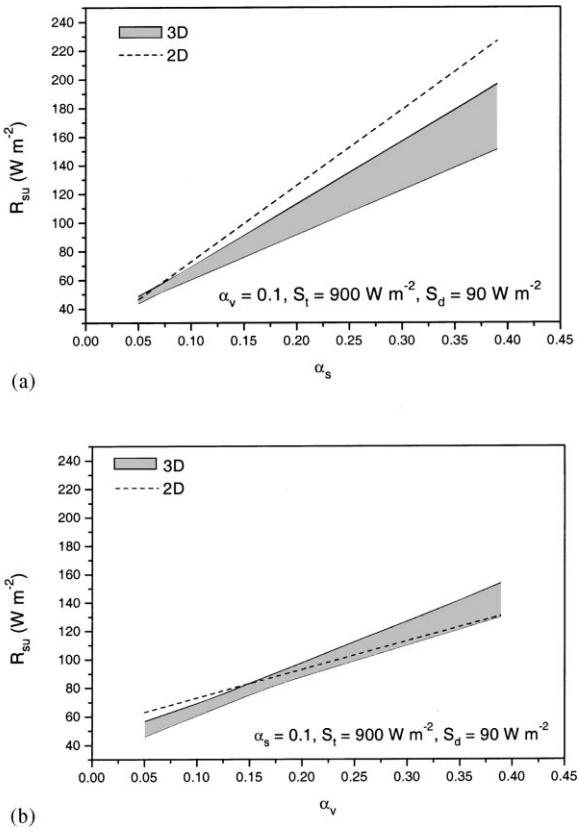


Fig. 6. Range in the modeled upwelling shortwave radiation, $R_{su.3D}$, of the 100 randomly-placed simulated radiometer locations versus varying reflection coefficient of (a) soil ($\alpha_s$) and (b) vegetation ($\alpha_v$). The 2-D estimate of $R_{su.2D}$ is shown as a dashed line.

The spatial variability of the upwelling radiation increased when soil radiative properties (i.e. radiative temperature, reflection coefficient) were larger then vegetation radiative properties, because radiation from the soil is blocked from reaching a radiometer by the surrounding vegetation. Vegetation contributions to upwelling radiation are also intercepted, but are replaced by contributions from foliage with similar radiative properties. For plants with a low height to distance ratio (e.g. lower canopy height with similar stand density), the amount of radiation blocked by the 3-D structure will usually be less than in our example, leading to smaller differences between the 2-D and 3-D estimates of $R_u$.

The uncertainty in an estimate of $R_n$ from a single measurement location depends on the vegetation distribution around the measurement location. In our simulations, the uncertainty was less than ∼10% of $R_n$ even for conditions with large differences in the surface properties. For periods when there is significant shading (i.e., early morning hours, late afternoon, and seasons with low solar elevation), differences in radiative temperatures of the ecosystem components are probably small, and the uncertainty in the estimate of net radiation from one measurement location will also be small.

For vegetation with a closed-canopy, less variation in the upwelling components of $R_n$ than we simulated here is expected, since vegetation structure is spatially more homogeneous and differences of surface radiation temperatures of the ecosystem components are most likely small. Nevertheless, Droppo and Hamilton (1973) detected up to 13% differences in midday net radiation above a deciduous forest when measured from three towers located only ∼15 m apart. They surmised that the difference in $R_n$ between locations was due to spatial variation in the vegetation structure around the measurement locations.

Smith et al. (1997) carefully intercalibrated net radiometers of different models, and found a ∼16% range of variation in measured $R_n$ between sensors. Our measurements and modeling suggest that in open-canopy ecosystems, spatial variation in upwelling radiation components are comparable in magnitude to uncertainties in net radiometer responses. Consequently, the uncertainty in the estimation of net radiation for an open-canopy ecosystem makes it difficult to validate the accuracy of the eddy covariance method by determining the achievement of energy closure.

## 4. Conclusions

The three dimensionality of a forest canopy has a large impact on estimating upwelling longwave radiation from measured surface radiation temperature of ecosystem components. An estimate of upwelling radiation using simple cover fraction scaling (the 2-D approach) can be significantly different from the upwelling radiation estimated by taking into account the three dimensional structure of the canopy. This difference occurs because part of the radiation emitted or reflected from the forest floor is intercepted by vegetation. Despite this radiative energy input to foliage, that supplements foliar interception of downwelling radiation, we found that radiative temperatures of juniper foliage were lower than radiative temperatures of soil on cloudless summer days. This is probably a consequence of the good coupling of the juniper leaves to the atmosphere and the ability of the plant to also lose energy as latent heat by transpiring water drawn from deep soil reserves.

Taking into account the change in vegetation fraction with viewing angle improves an estimate of the upwelling radiation at a radiometer location over the simple orthogonal cover fraction estimate. If vegetation parameters ($k$ and LAI) are known accurately, it is possible to estimate the average upwelling radiation from radiation measurements made separately above the major ecosystem components (e.g., soil and vegetation). Adjustments for shade and sunlit fractions need to be made depending on sun position.

The upward radiation received by a single radiometer placed above an ecosystem depends on the distribution of the vegetation and soil around the instrument location and on the surface properties of the soil and vegetation that are in the field of view of the radiometer. The spatial variation is generally increased if surface properties ($T_r$ and $\alpha$) differ between the ecosystem components (i.e. soil and overstory). The variability is largest when the radiative flux from the ground is larger than the flux from the canopy, since it is the ground contributions that are intercepted by the canopy vegetation; radiation from the canopy that is intercepted is replaced by radiation from foliage with

similar properties. We conclude that at our site the measured upwelling component of the net radiation depends on measurement location but differs from the mean upwelling radiation by less than 10% even for large differences in $T_r$ and $\alpha$ of the ecosystem components. This uncertainty is not enough to explain the lack of energy closure in this ecosystem. Further investigation should focus on quantifying loss of energy by advective processes, and determining the uncertainties and representativeness of measured turbulent fluxes of sensible and latent heat in the heterogeneous environment of this open canopy (Schmid and Lloyd, 1999).

## Acknowledgements

This study was funded by NASA (grant #NAGW-4436 and #NAG5-7551). We are grateful to Will Hutchinson for his field assistance. We gratefully acknowledge the assistance of Teal Purrington from the Bureau of Land Management (BLM) in site selection. We thank Richard and Doris Waring for their help in establishing the study site. We thank Dr. Ronald Dobosy for his valuable comments on various aspects on aircraft-tower intercomparison of net radiation.

## References

Blanken, P.D., Black, T.A., Yang, P.C., Neumann, H.H., Nesic, Z., Staebler, R., den Hartog, G., Novak, M.D., Lee, X., 1997. Energy balance and canopy conductance of a boreal aspen forest: partitioning overstory and understory components. J. Geophys. Res. 102, 28915–28927.

Blyth, E.M., Harding, R.J., 1995. Application of aggregation models to surface heat flux from the Sahelian tiger bush. Agric. For. Meteorol. 72, 213–235.

Desjardins, R.L., Macpherson, J.I., Mahrt, L., Schuepp, P.H., Pattey, E., Neumann, H., Baldocchi, D.D., Wofsy, S., Fitzjarrald, D., McCaughey, H., Joiner, D.W., 1997. Scaling up flux measurement for the boreal forest using aircraft-tower combinations. J. Geophys. Res. 102 (D24), 29125–29133.

Dirmhirn, I., Belt, G.H., 1971. Variation of albedo of selected sagebrush range in the intermountain region. Agric. Meteorol. 9, 51–61.

Dolman, A.J., 1993. A multiple-source land surface energy balance model for use in general circulation models. Agric. For. Meteorol. 65, 21–45.

Droppo, J.G., Hamilton, H.L., 1973. Experimental variability in the determination of the energy balance in a deciduous forest. J. Appl. Meteorol. 12, 781–791.

Fan, S.-M., Goulden, M.L., Munger, J.W., Daube, B.C., Bakwin, P.S., Wofsy, S.C., Amthor, J.S., Fitzjarrald, D.R., Moore, K.E., Moore, T.R., 1995. Environmental controls on the photosynthesis and respiration of a boreal lichen woodland: a growing season of whole-ecosystem exchange measurements by eddy correlation. Oecologia 102 (4), 443–452.

Garratt, J.R., 1978. Transfer characteristics for a heterogeneous surface of large aerodynamic roughness. Q. J. R. Meteorol. Soc. 104, 491–502.

Goulden, M.L., Munger, J.W., Fan, S.-M., Daube, B.C., Wofsy, S.C., 1996. Measurements of carbon sequestration by long-term eddy covariance: methods and critical evaluation of accuracy. Global Change Biol. 2, 169–182.

Gower, S.T., Vogel, J.G., Norman, J.M., Kucharik, C.J., Steele, S.J., Stow, T.K., 1997. Carbon distribution and aboveground net primary production in aspen, jack pine, and black spruce stands in Saskatchewan and Manitoba, Canada. J. Geophys. Res. 102 (D24), 29029–29041.

Grelle, A., 1997. Long-term water and carbon dioxide fluxes from a boreal forest. Ph.D. Thesis, Swedish University of Agricultural Sciences, Uppsala, Sweden.

Gritz, L., Hahn, J.K., 1996. BMRT: a global illumination implementation of the RenderMan standard. J. Graphic Tools 1 (3), 29–47.

Hipps, L.E., 1989. The infrared emissivities of soil and *Artemisia tridentata* and subsequent temperature corrections in a shrub-steppe ecosystem. Remote Sensing Environ. 27, 337–342.

Huband, N.D.S., Monteith, J.L., 1986. Radiative surface temperature and energy balance of a wheat canopy. Boundary-Layer Meteorol. 36, 1–17.

Humes, K.S., Kustas, W.P., Moran, M.S., Nichols, W.D., Weltz, M.A., 1994. Variability of emissivity and surface temperature over a sparsely vegetated surface. Water Resourc. Res. 30 (5), 1299–1310.

Jones, H.G., 1992. Plants and Microclimate: a Quantitative Approach to Environmental Plant Physiology. Cambridge University Press, UK.

Kelliher, F.M., Köstner, B.M.M., Hollinger, D.Y., Byers, J.N., Hunt, J.E., McSeveny, T.M., Mesert, R., Weir, P.L., Schulze, E.-D., 1992. Evaporation, xylem sap flow and tree transpiration in a New Zealand broad-leaved forest. Agric. For. Meteorol. 62, 53–73.

Laubach, J., Raschendorfer, M., Kreilein, H., Gravenhorst, G., 1994. Determination of heat and water vapour fluxes above a spruce forest by eddy correlation. Agric. For. Meteorol. 71, 373–401.

Law, B.E., Waring, R.H., 1994. Combining remote sensing and climatic data to estimate net primary production across Oregon. Ecol. Appl. 4 (4), 717–728.

Lee, X., Black, T.A., 1993. Atmospheric turbulence within and above a Douglas-fir stand Part II. Eddy fluxes of sensible heat and water vapour. Boundary-Layer Meteorol. 64, 369–389.

McCaughey, J.H., Laufleur, P.M., Joiner, D.J., Bartlett, P.A., Jelinski, D.E., Ryan, M.G., 1997. Magnitudes and seasonal patterns or energy, water, and carbon exchanges at a boreal young jack pine forest in the BOREAS northern study area. J. Geophys. Res. 102 (D24), 28997–29907.

Monteith, J.L., Unsworth, M.H., 1990. Principles of Environmental Physics. Edward Arnold, Hodder Headline PLC, London.

Norman, J.M., Kustas, W.P., Humes, K.S., 1995. Source approach for estimating soil and vegetation energy fluxes in observations of directional radiometric surface temperature. Agric. For. Meteorol. 77, 263–293.

Paw U, K.T., 1992. Development of models for thermal infrared radiation above and within plant canopies. ISPRS J. Photogrammetry Remote Sensing 47, 189–203.

Runyon, J., Waring, R.H., Goward, S.N., Welles, J.M., 1994. Environmental limits on net primary production and light-use efficiency across the Oregon transect. Ecol. Appl. 4, 226–237.

Schmid, H.P., 1997. Experimental design for flux measurements: matching scales of observations and fluxes. Agric. For. Meteorol. 87, 179–200.

Schmid, H.P., Lloyd, C.R., 1999. Spatial representativeness and the location bias of flux footprints over inhomogeneous areas. Agric. For. Meteorol. 93, 195–209.

Schwerdtfeger, P., 1976. Physical principles of micro-meteorological measurements. Development in Atmospheric Science. Elsevier, Amsterdam.

Shuttleworth, W.J., Wallace, J.S., 1985. Evaporation from sparse crops — an energy combination theory. Q. J. R. Meteorol. Soc. 111, 839–855.

Smith, E.A., Hodges, G.B., Bacrania, M., Cooper, H.J., Owens, M.A., Chappel, R., Kincannon, W., 1997. BOREAS net radiometer engineering study. NASA Contractor Report (NASA Grant NAG5-2447), NASA-Goddard Space Flight Center, Greenbelt.

Unsworth, M.H., Monteith, J.L., 1975. Long-wave radiation at the ground I. Angular distribution of incoming radiation. Q. J. R. Meteorol. Soc. 101, 13–24.